3-D Printed Bandpass Filters With Coupled Vertically Extruded Split Ring Resonators

Andrea Vallecchi, Darren Cadman, William G. Whittow, *Senior Member, IEEE*, John Vardaxoglou, *Fellow, IEEE*, Ekaterina Shamonina, and Christopher J. Stevens, *Member, IEEE*

***Abstract*— The additive manufacturing process of multimaterial extrusion offers performance advantages using functional materials including conductors while making accessible the third dimension in the design of electronics. In this work, we show that the additional geometrical freedom offered by this technique can be exploited for the design and realization of filters made of 3-D resonators that exhibit enhanced characteristics. The coupling properties of 3-D grounded square split ring resonators (SRRs) are initially explored. We demonstrate by simulations and experiments that SRRs with finite height display significantly stronger coupling compared to equivalent thin printed circuit structures. The observed trend can be exploited for designing filters with wider operational bandwidths for a given footprint, or miniaturized layouts and enhanced compatibility with fabrication limits for minimum feature size and spacing without performance degradation. This concept is demonstrated by presenting results of full-wave simulations for sample bandpass filters with identical footprint but formed by coupled 3-D square SRRs of different heights, showing that filters with taller resonators exhibit increasingly wider bandwidths. Two filter prototypes with center frequencies at 1.6 and 2.45 GHz are manufactured by multimaterial 3-D printing. The measured characteristics of these prototypes are found to be in good agreement with numerical simulations taking into account the effect of the lossier metallic and dielectric materials used in 3-D printing and confirm the predicted larger bandwidth of the filters made of 3-D SRRs with marginally higher insertion losses.**

***Index Terms*— Additive manufacturing, direct digital manufacturing (DDM), electromagnetic coupling, filter design, fused deposition modeling (FDM), resonance, split-ring resonators, 3-D printing.**

I. Introduction

THE advancement of additive manufacturing technology has recently produced a new generation of 3-D printing techniques and materials that enable the realization of complex geometries containing both metals and dielectrics [1]. These capabilities can address the requirements of 3-D electromagnetic designs incorporating nonplanar composite structures and nonhomogeneous materials. Single material additive manufacturing has found application in the realization of many microwave and millimeter-wave devices, including metamaterials [2]–[4], horn and patch antennas [5]–[7], graded index and Luneburg lenses [8]–[10], frequency selective surfaces [11], [12], and and microwave filters [13], [14].

A strong advantage of using additive manufacturing to print filters is the possibility to implement 3-D miniaturization techniques, such as folding and stacking methods. In fact, at RF and low microwave frequencies, it may be desirable to make filters as small as possible for application in portable electronic equipment, particularly wearable electronics, and the cost-effective use of large scale integrated chip wafers commonly employed for all RF circuitry in the intermediate frequency and baseband section. To achieve miniaturization, filters can be constructed using lumped or quasi-lumped elements. One effective method for the miniaturization of coupled split ring resonator (SRR) filters is to add capacitive loading to the resonators via capacitors connected in series across the resonator gaps. Increasing the capacitor values can decrease the size of resonators. However, the smaller the resonators, the closer they need to be spaced in order to reach the same coupling coefficient, imposing more severe fabrication tolerances, and the harder it could be to achieve the required external quality factors [15].

The additional geometrical freedom (height) in the design of coupled resonators provided by 3-D printing can be effectively exploited for designing filters with enhanced characteristics, where miniaturization is achieved without sacrificing performance. In this article, the coupling between 3-D raised square SRRs amenable to fabrication with 3-D printing techniques is investigated, showing that a significant increase in coupling can be achieved with respect to a thin PCB resonator structure by raising the height of the rings. The possibility of exploiting such stronger coupling for designing bandpass filters with wider fractional bandwidth is then illustrated by presenting simulated results for a few sample filter structures made of SRRs with different heights. Preliminary results related to this part of the work have been presented in [16].

The manufacturing of two bandpass filter prototypes with center frequencies at 1.6 and 2.45 GHz using a multimaterial extrusion-based 3-D printer is then described. Fused deposition

Manuscript received December 26, 2018; revised March 25, 2019 and June 6, 2019; accepted June 23, 2019. Date of publication September 17, 2019; date of current version November 5, 2019. This work was supported by the U.K. Engineering and Physical Science Research Council (EPSRC) through the Project "Synthesizing 3-D Metamaterials for RF, Microwave and THz Applications" under Grant EP/N010493/1. *(Corresponding author: Andrea Vallecchi.)*

A. Vallecchi, E. Shamonina, and C. J. Stevens are with the Department of Engineering Science, University of Oxford, Oxford, OX1 3PJ, U.K. (e-mail: andrea.vallecchi@eng.ox.ac.uk; ekaterina.shamonina@eng.ox.ac.uk; chris.stevens@eng.ox.ac.uk).

D. Cadman, W. G. Whittow, and J. Vardaxoglou are with the Wolfson School of Mechanical, Electrical and Manufacturing Engineering, Loughborough University, Loughborough, LE11 3TU, U.K. (e-mail: d.a.cadman@lboro.ac.uk; w.g.whittow@lboro.ac.uk; j.c.vardaxoglou@lboro.ac.uk).

Color versions of one or more of the figures in this article are available online at http://ieeexplore.ieee.org.

Digital Object Identifier 10.1109/TMTT.2019.2934456

modeling (FDM) utilizes extrusion of thermoplastic materials through a heated nozzle. Until recently, it was only applied to the production of mechanical components and solid models but is now being used for electronics [17], [18]. This has largely been facilitated by the development of new filaments that offer more than merely structural properties. In particular, the use of FDM for electronics is enabled by compatible conductive filament materials and inks. The Voxel8 (V8) Developers Kit offers a direct digital manufacturing (DDM) platform that has an FDM nozzle alongside V8 silver microparticle ink for metal 3-D printing, which is dispensed by a syringe using a high pressure pneumatic pump and cures almost immediately at room temperature, with no postprocessing step required. The V8 silver ink is specified with a conductivity just an order of magnitude lower than that of copper [19], and thus high enough for high performance antennas and RF devices. Another conductive filament for FDM named Electrifi, consisting of a polyester and copper composite, has also been recently introduced which has the advantage of being compatible with most of the commercially available desktop filament-based 3-D printers. However, the conductivity of this filament is significantly lower than that of V8 ink [20]. A broader selection of dielectric filaments is available for FDM.

Most commonly used are the standard thermoplastics such as acrylonitrile butadiene styrene (ABS), polycarbonate (PC), and polyetherimide (PEI) also known as ULTEM resin, which have similar characteristics, and polylactic acid (PLA) which has a higher loss tangent [21], [22]. Higher permittivity FDM compatible materials have been also developed as low-loss ceramic-thermoplastic composites [10], [22], [23]. However, at present, filaments explicitly developed for creating parts for microwave applications are scarce and data for the batch-to-batch variation in dielectric properties of available filaments are unavailable. In addition, there is the factor of variation in print quality between printer types that can affect the resulting printed microwave structures. The filter prototypes presented here have been manufactured using DDM on V8 dual material 3-D printer with one nozzle extruding standard PLA filaments (essentially FDM) and the second extruding V8 silver ink.

The organization of the work is as follows. In Section II, the coupling properties of 3-D square SRRs on a grounded dielectric substrate, amenable to contextual fabrication with 3-D printing, are explored by both simulations and experiments. Next, sample designs of bandpass filters made of coupled 3-D square SRRs of different heights are presented in Section III. The fabrication of two different filter prototypes by DDM is described in Section IV, where the measured characteristics of the realized filters are also discussed and compared with results of simulation taking into account the effect of the lossy characteristics of metallic and dielectric materials used in DDM.

II. Coupling of 3-D SRRs

Microstrip SRRs are commonly used for filter design [15]. Raised versions of the thin SRRs that can be easily realized by 3-D printing are considered in this work. Fig. 1 shows the trend of the resonance frequency, f_r, and quality factor, Q, of these

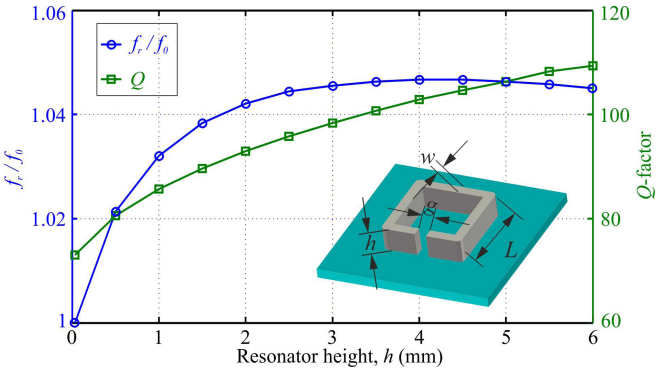

Fig. 1. Resonance frequencies f_r and quality factors Q against height h of the 3-D SRR above a grounded dielectric substrate shown in the inset. f_r is normalized with respect to the resonance frequency of the planar microstrip element ($h = 0.035$ mm). SRR dimensions are: $L = 20$, $w = 1.626$, and $g = 1$ mm. The dielectric substrate is 1.6 mm thick and its permittivity is $\epsilon_r = 2.5$ with $\tan\delta = 0.001$. Results are obtained from full-wave simulations with CST MWS of the driving point impedance of the SRR fed at the gap.

TABLE I

Reference Dimer Configurations Considered in the Numerical and Experimental Investigation of the Coupling Properties of 3-D Raised Square SRRs. The Pair of SRRs With Different Orientations Are Separated by the Same Spacing

Far	Up-down	Near	Up-up	Left-left
				

3-D SRRs, whose structure is shown in the inset of the figure, for variable resonator height h. f_r and Q are obtained via simulation of the driving point impedance of the SRR fed at the gap with the EM software CST Microwave Studio (MWS). Frequencies are normalized with respect to the resonance frequency f_0 of the thin SRR ($h = 0.035$ mm). It is clear that the self-resonance frequency of the resonators increases with height initially, with a maximum value at between 4 and 5 mm thick. This occurs because, while the self-inductance (L) of the resonator falls logarithmically with height, the capacitance (C) arising from the gap and surfaces of the SRR rises near linearly, eventually more than compensating for the reduced inductance in $f_r = 1/\sqrt{LC}$. At the same time, the quality factor increases as a result of the resistance of the SRR decreasing logarithmically for increasing height at a faster rate than its inductance [24].

Next, the coupling properties of 3-D raised square SRRs are examined by simulations and experimentally. For illustration purposes, the set of typical configurations of a pair of coupled 3-D SRRs shown in Table I, where the SRRs have different orientations but are separated by the same fixed spacing, is analyzed.

As explained in [15], different arrangements of the SRR dimer exhibit distinctive coupling characteristics associated with the particular configurations of the electric and magnetic fields between the resonators. However, the overall coupling

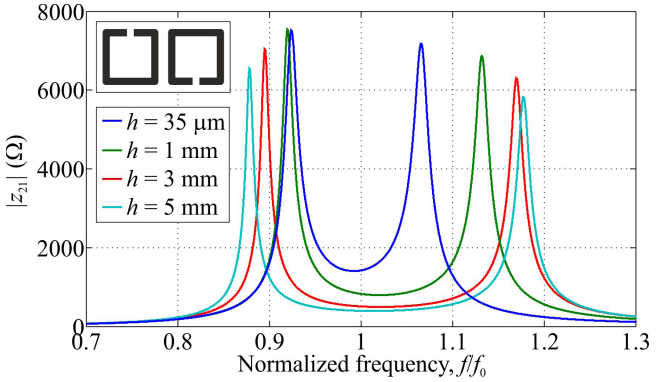

Fig. 2. Magnitude of the transfer impedance z_{21} as simulated with CST MWS for the sample "up-down" SRR dimer configuration shown in the inset at variable resonator height $h = 0.035, 1, 3, 5$ mm. The SRRs are placed on top of a 1.6-mm-thick PLA substrate with permittivity $\epsilon_r = 2.5$ and $\tan\delta = 0.01$. z_{21} is shown against the frequency normalized with respect to the resonance frequency f_0 of the corresponding single isolated thin SRR ($h = 0.035$ mm).

coefficient can be simply extracted using the formula

$$\kappa = \frac{f_l^2 - f_h^2}{f_l^2 + f_h^2} \tag{1}$$

where f_h and f_l represent the higher and lower resonance frequencies of the coupled structure. These latter can be easily identified by inspection of the magnitude of the simulated transfer impedance z_{21} plotted against frequency, which for sufficiently strong coupling exhibits distinct peaks at the resonances of the hybridized modes of the coupled SRRs. The characteristic trend of z_{21} for sample pairs of SRRs with opposite vertical orientation ("near" configuration) is illustrated in Fig. 2 for variable resonators height.

In particular, as shown in Fig. 1, the dimensions of the SRRs were chosen to match those of reference copper SRRs fabricated by mechanically slicing a square copper pipe, and cutting a vertical slit along the pipe slice to form the resonator gap, which have been used in the preliminary experiments conducted to confirm simulation results relative to coupling. These copper SRRs have external side length $L = 20$ mm, conductor width $w = 1.626$ mm, and gap width $g = 1$ mm, while their height is varied from the thin case $h = 0.035$ mm to $h = 5$ mm. The SRRs are placed on a 1.6-mm-thick grounded PLA substrate with permittivity $\epsilon_r = 2.5$ and $\tan\delta \approx 0.01$ at a separation distance between their adjacent faces of 0.5 mm. The resonance of the isolated SRRs occurs at about 1.5 GHz. The evolution of f_l and f_h for varying SRR height retrieved from the simulation of z_{21} for four different dimer configurations is summarized in Fig. 3. In general, we expect magnetic coupling to be approximately the same between the four dimer configurations "far", "up-down", "near", "up-up", and "left-left".

The upper resonance in Fig. 3(a) increases monotonically with h for all dimer configurations, while in contrast, the lower resonance trend shown in Fig. 3(b) varies with the configuration. These features are the results of the near-field coupling through the charge and current distributions on the SRRs, or, in other terms, between the equivalent electric and magnetic dipole moments of the SRRs. Key, here, is the

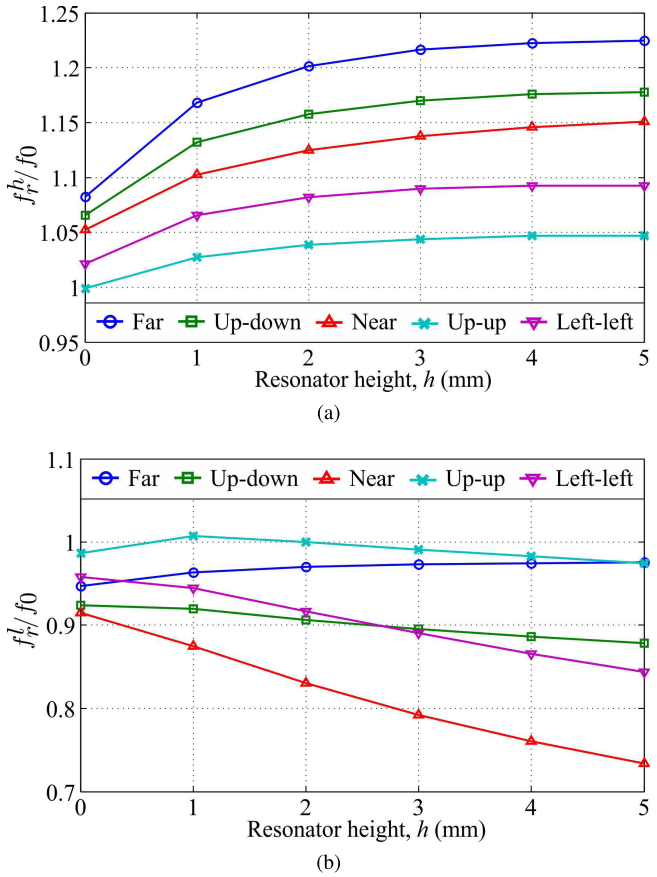

Fig. 3. (a) Higher and (b) lower resonance frequencies for the four coupled SRR dimer configurations given in Table I at variable resonator height $h = 0.035, 1, 2, 3, 4, 5$ mm. Data are normalized with respect to the resonance frequency f_0 of the corresponding single thin SRR ($h = 0.035$ mm) and are obtained by inspection of the magnitude of the transfer impedance z_{21} of the various dimer configurations simulated with CST MWS.

strength and sign of these two types of interaction, which can oppose or reinforce each other depending on the relative orientation of the SRRs. A comprehensive description of the coupling mechanisms between the SRRs would require an analysis similar to that in [25], which, however, is beyond the scope of the present work. The focus, here, is on the overall coupling coefficient of a pair of SRRs, calculated by means of (1) and the resonance frequency data provided in Fig. 3, which is presented in Fig. 4.

The latter graph shows that the raised SRRs exhibit significantly stronger coupling compared to the thin structures and that their coupling coefficient steadily increases with their height in most of the configurations. Only in the "far" configuration, coupling tends to saturate for $h \geq 4$ mm. In fact, in this arrangement, the SRR gaps, where the electric field concentrates, are far apart and the electric interaction is weak; as a result, coupling between the SRRs is predominantly due to the magnetic field, which for taller resonators can grow stronger, but also become more confined inside them. We expect this to result in an eventual drop in coupling for this case as height is further increased.

Experiments have been conducted to validate the simulation results in Fig. 4. Our method for measuring the SRR coupling

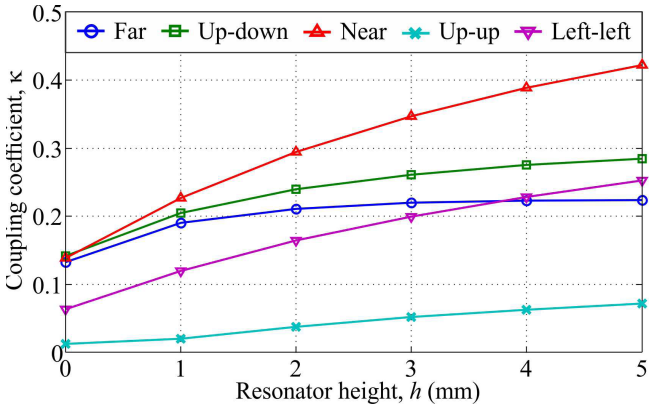

Fig. 4. Coupling coefficients of the 3-D SRR dimer configurations analyzed for variable resonator height $h = 0.035, 1, 2, 3, 4, 5$ mm, as calculated with (1) using the simulation data in Fig. 3.

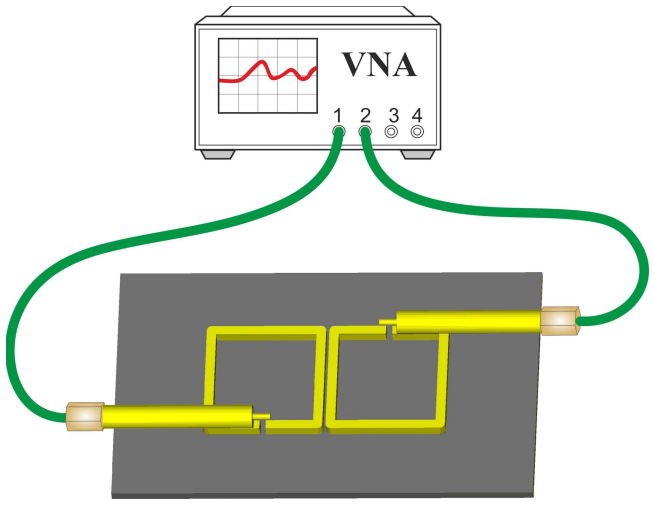

Fig. 5. Experimental setup for the measurement of the SRR coupling where two electric probes are used to excite the SRRs.

is shown in Fig. 5. Each resonator is excited by an electric dipole probe connected to one of the two ports of a vector network analyzer (VNA). These dipoles are placed so as to couple to the electric fields in the split-ring gaps. In the presence of the specimens, the transmission scattering parameter s_{21} between the two probes measured with the VNA exhibits two peaks at the resonance frequencies of the coupled SRRs. Direct coupling of the probes was preliminary recorded with the VNA and then subtracted from the measurement of each dimer configuration. An adhesive polymer spacer was used to fix the SRRs parallel to each other at 0.5-mm separation between their faces and the responses of different dimers were measured for $h = 1, 2, 3, 4, 5$ mm. The raw s_{21} data have been analyzed to obtain the upper and lower resonances for the various dimer configurations, and the coupling coefficients gathered from those data are presented in Fig. 6. There is a clear trend of measured results consistent with the simulations in Fig. 4 and the two sets of data also agree well quantitatively. It is, thus, very clear that the height of raised SRRs can provide direct control on the strength of coupling between resonators.

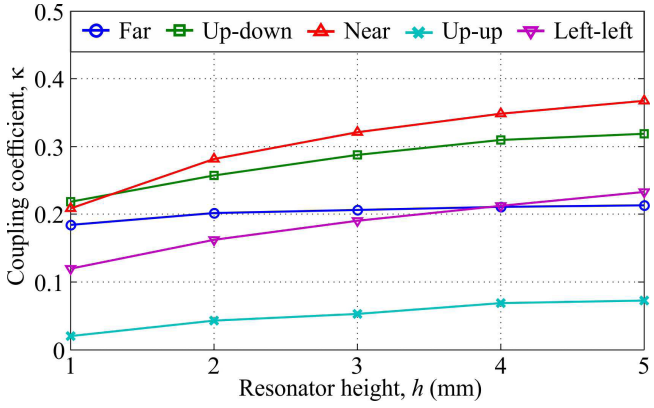

Fig. 6. Coupling factor of different 3-D SRR dimer configurations given in Table I at variable height of the SRRs ($h = 1, 2, 3, 4, 5$ mm) measured with the apparatus in Fig. 5.

This additional degree of freedom in tailoring the geometry of resonators can be exploited in several ways.

1) The increased coupling enables larger bandwidth than possible with thin PCB-based filters for the same overall footprint and minimum feature sizes.
2) In 3-D fabrication, minimum feature sizes and spacings are a strong constraint on the design of a structure making it impossible to place resonators very close together— building them upward instead permits greater coupling than would otherwise be possible.
3) Since we are at liberty to design resonators of different heights, it is possible to envisage filters where variable couplings between resonators are all achieved by varying their relative heights. One may even imagine resonators whose height is tapered in the direction along the substrate resulting in very fine control of individual couplings without compromising the minimum gap and feature size limits.

The widening of filter passband with an increment of the coupling between the resonators can be estimated by referring to the classical theory of filters with inline coupling topology [15], [26]. In particular, the transmission coefficients of an nth order bandpass coupled resonator filter, with center frequency f_0 and passband-edge frequencies f_1 and f_2, corresponding to a fractional bandwidth FBW $= (f_2 - f_1)/f_0$, can be expressed in terms of the external quality factors Q_{ei}, $i = 1, n$, and coupling matrix $[K] = [\kappa_{ij}]$, which is a reciprocal $n \times n$ matrix, as

$$s_{21} = \frac{2}{\text{FBW}\sqrt{Q_{e1}Q_{en}}}[A]^{-1}_{n1} \tag{2}$$

with $[A]$ denoting the matrix

$$[A] = [q] + p[U] - \text{jFBW}^{-1}[K] \tag{3}$$

where p is the complex low-pass frequency variable, $p = j/\text{FBW}(f/f_0 - f_0/f)$, $[U]$ is the $n \times n$ identity matrix, and $[q]$ is an $n \times n$ matrix with all entries zero except for $q_{11} = 1/(Q_{e1}\text{FBW})$ and $q_{nn} = 1/(Q_{en}\text{FBW})$. The external quality factors and the coupling coefficients can be related to the coefficients g_i, $i = 0, 1, 2, \ldots n$, of the low-pass prototype

filter with the specified response and cutoff frequency Ω_c through the relations

$$Q_{e1(n)} = \frac{g_{0(n)} g_{1(n+1)} \Omega_c}{\text{FBW}} \qquad \kappa_{ij} = \frac{\text{FBW}}{\Omega_c \sqrt{g_i g_j}}. \tag{4}$$

These formulas are approximate and their accuracy improves when the fractional bandwidth narrows [26], but can serve the purpose of qualitatively assessing the trend and interdependence of the parameters controlling the response of an inline coupling filter. For simplicity, we will assume that all the resonators are tuned to the passband center frequency f_0, and that each resonator is coupled only with the two adjacent elements; the two terminal resonators are coupled with just one neighbor resonator and one of the two filter ports. A reference fourth-order ($n = 4$) bandpass Butterworth filter is specified to have center frequency $f_0 = 1.6$ GHz, with 10% FBW. The low-pass prototype parameters, given for a normalized low-pass cutoff frequency $\Omega_c = 1$ rad/s, are $g_0 = g_5 = 1.0$, $g_1 = g_4 = 0.7654$, $g_2 = g_3 = 1.8478$. The required nominal external quality factors, Q^0_{e1} and Q^0_{e4}, and coupling coefficients $\kappa^0_{12} = \kappa^0_{34}$ and κ^0_{23} can be derived by (4). Inspection of Fig. 4 reveals that for all considered dimer configurations, except the "far" but including the "up-down", which is widely used in inline filters, strength of coupling between the taller SRRs is more than double than that in the thin structure; moreover, results in Fig. 1 show that Q when $h = 6$ mm is about 1.5 times greater than that for a thin SRR. The theoretical transmission coefficients of the considered filter calculated by using (2) for the nominal values of the coupling coefficients and external quality factors, $\kappa^0_{i,i+1}$, $i = 1, 2, 3$, and Q^0_{ej}, $j = 1, 4$, and when these quantities simultaneously undergo sample increases of up to a factor of 2 and 1.4, respectively, are shown in Fig. 7. As expected, the larger coupling between the filter elements results in a significant enlargement of the passband width, although this is accompained by a more pronounced ripple, which is mainly ascribable to the higher external quality factors. However, as it will be shown in Section II, the filter structure can be tweaked to recover good impedance matching and negligibly small ripple across the passband only minimally sacrifying the improvement in bandwidth provided by the stronger coupling.

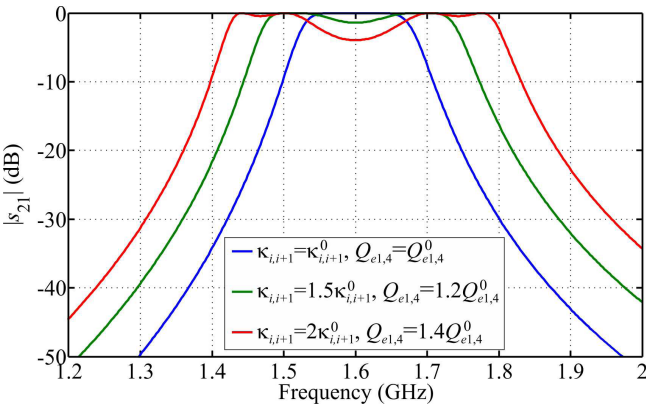

Fig. 7. Theoretical transmission coefficient of a fourth-order filter with Butterworth response for increasing coupling κ_{ij} and external quality factors Q_e.

III. Sample Filter Designs with Coupled 3-D SRRs

Three simple bandpass filters made of coupled 3-D square SRRs of different heights have been developed, using the coupling matrix method [15], to explore the capability offered by height variation in design. The first set of filters have been designed to operate at a central frequency of 1.6 GHz. The initial planar microstrip version of the filter was tailored by simulation to have a passband width of $\simeq$150 MHz, maximum passband attenuation of 1 dB, stopband attenuation of 20 dB, and stopband width of $\simeq$400 MHz (i.e., transition bands $\simeq$125 MHz). A fourth-order filter structure was used to achieve these specifications. The central frequency of operation and the choice of a 1.6-mm-thick grounded dielectric substrate with permittivity $\epsilon_r = 2.26$ (e.g., polyethylene) substantially dictate the size of the SRRs, which are set up have side length $L = 20$ mm for a conductor width $w = 1.6$ mm (see Fig. 1). The width of the SRR gaps and the interelement distances has been assumed as the remaining design parameters that need to be adjusted to accomplish the desired filter performance. The antisymmetric layout of the reference filter model with planar copper SRR elements ($h = 0.035$ mm) is shown in Fig. 8(a): the central SRRs have 0.8-mm-wide gaps and are separated by a 1.8 mm spacing, while for the external elements the gap width is 2.9 mm and the separation from the adjacent SRR is 0.9 mm. The transmission coefficient (s_{21}) of this reference planar microstrip filter is plotted in Fig. 8(b), where to substantiate the theoretical results shown in Fig. 7, the simulated effect of raising the height of resonators, while keeping the rest of the filter dimensions unchanged, is also shown. This graph reveals that bandwidth enhancements consistent with theoretical predictions can be achieved as a consequence of the stronger coupling between the raised SRRs, while increase in passband attenuation due to deterioration of impedance matching at the ports appears limited ($\simeq$2 dB for $h = 4$ mm). This is likely due to the fact that the external quality factors Q_e grows less with SRR height than the Q of an isolated resonator in Fig. 1 because of the interaction with the adjacent internal element possibly contributing to strengthen the coupling of the external SRRs to the filter ports.

Then, two additional designs using 3-D square SRRs with height $h = 2$ and $h = 4$ mm have been created to confirm feasibility of meeting the specification initially set for passband attenuation across broader bandwidths. These two filters have layouts very similar to the reference planar one, from which they are derived with minimal adjustments of their feed lines positions, sizes of the SRR gaps, and distance between the elements to optimize their responses and restore good impedance matching at the input ports. The performance of these filters has been initially assessed assuming that the resonators were made of copper and printed on the same low loss substrate that could be used for planar filters. Then, the designs with the raised SRRs have been simulated to test the impact of using material properties for 3-D printed versions on their responses and compare with the measurements of

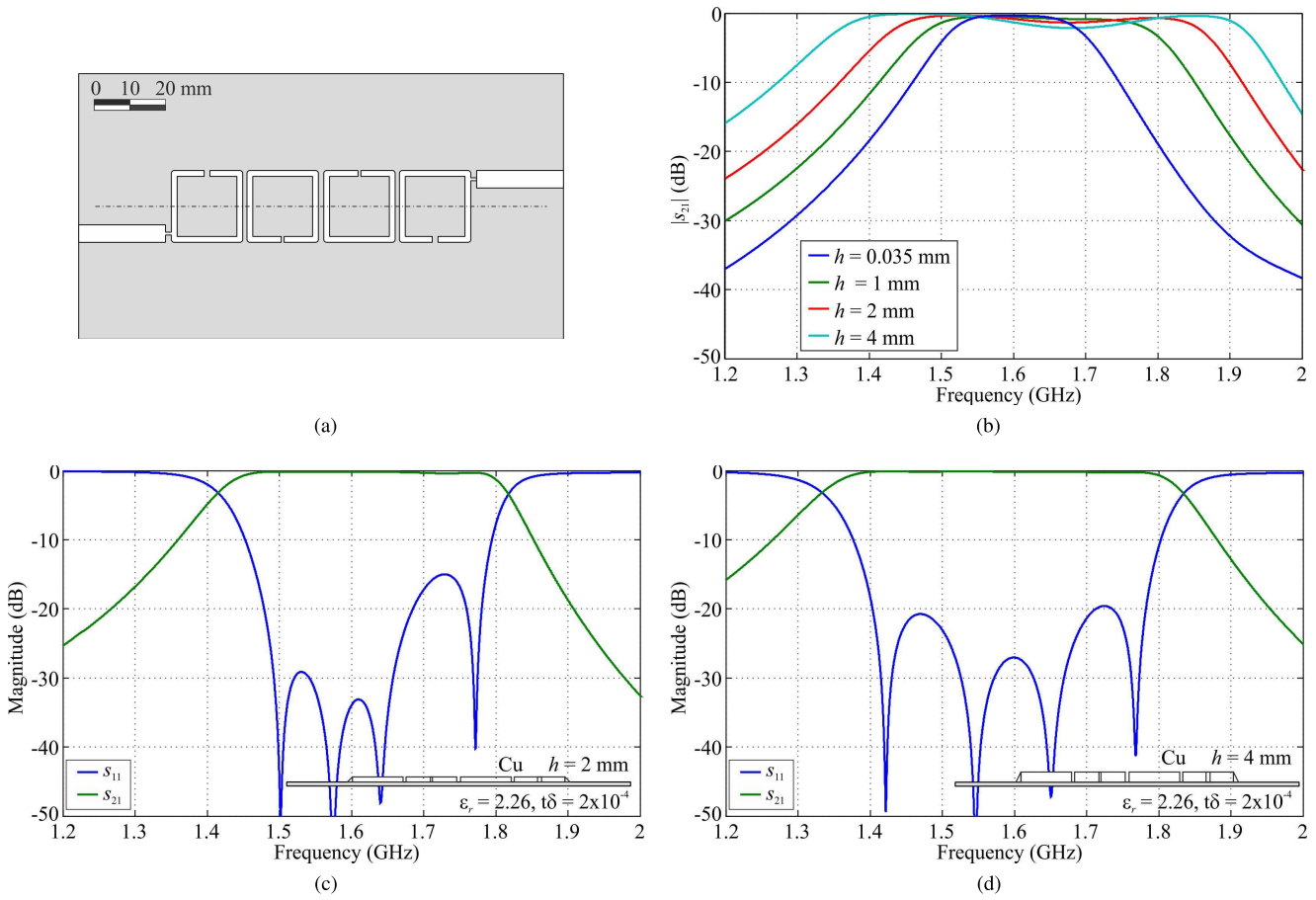

Fig. 8. Fourth-order bandpass filter made of coupled SRRs with center frequency at 1.6 GHz. The SRRs are assumed to be made of copper (Cu) and printed on a substrate with $\epsilon_r = 2.26$ and $\tan\delta = 2 \times 10^{-4}$. (a) General layout. Filter response simulated with CST MWS is presented for different configurations: (b) transmission coefficient (s_{21}) of the reference thin PCB design ($h = 0.035$ mm) and its modification by raising the height of resonators while the rest of the filter dimensions is kept unchanged; reflection (s_{11}) and transmission (s_{21}) coefficients of 3-D versions of the filter with (c) 2-mm and (d) 4-mm-high resonators after reoptimization to restore the specified maximum insertion loss of 1 dB. Insets show the lateral views of the 3-D filter models.

TABLE II
MATERIAL PROPERTIES USED IN SIMULATIONS AND DESIGNS

Material Property	Model Value	3D Printed Value
Substrate material	Polyethylene	PLA
Substrate ϵ_r	2.26	2.35
Substrate $\tan\delta$	2×10^{-4}	10^{-2}
Substrate height (mm)	1.6	1.6
Conductor	Copper	Silver nanopaticle ink
Conductivity, σ (S/m)	5.96×10^7	2×10^6

TABLE III
FILTERS PERFORMANCE INDICES: CENTER FREQUENCY (f_0), BANDWIDTH (BW), FRACTIONAL BANDWIDTH (FBW), AND LOWER AND UPPER TRANSITION BANDS (TB_l AND TB_u)

h (mm)	f_0 (GHz)	BW (GHz)	FBW (%)	TB_l / TB_u (GHz)
0.035	1.6	0.13	8	0.150/0.141
2	1.62	0.35	22	0.176/0.111
4	1.59	0.44	28	0.224/0.147
0.035	2.45	0.1	4	0.175/0.145
2	2.44	0.29	12	0.197/0.135

fabricated prototypes, as reported in Section IV. Material properties for both the reference ideal filter and printed version are presented in Table II.

The simulated reflection and transmission responses of the 3-D SRR filter models assumed to be formed by copper SRRs on a low loss polyethylene substrate are shown in Fig. 8(c) and (d), respectively. These results highlight that the filters developed with the raised resonators, while having nearly identical footprints, exhibit dramatically wider passband widths for increasing resonator heights, with similar in-band attenuation and rolloff characteristics outside the passband as the reference thin PCB filter, as summarized in Table III. In this regard, it is noteworthy that extensive simulations performed as a cross-check by varying the relevant filter dimensions, consistently with given minimum feature size and separation constraints, have further confirmed that the bandwidth performance of the PCB filter cannot, indeed, be appreciably improved without failing to fulfill the requirement on insertion loss.

Next, in Fig. 9, a second filter example is presented to further explore the enhanced design flexibility associated with controlling the vertical extension of the resonators. Here, we are aiming at overcoming the limits presented by not

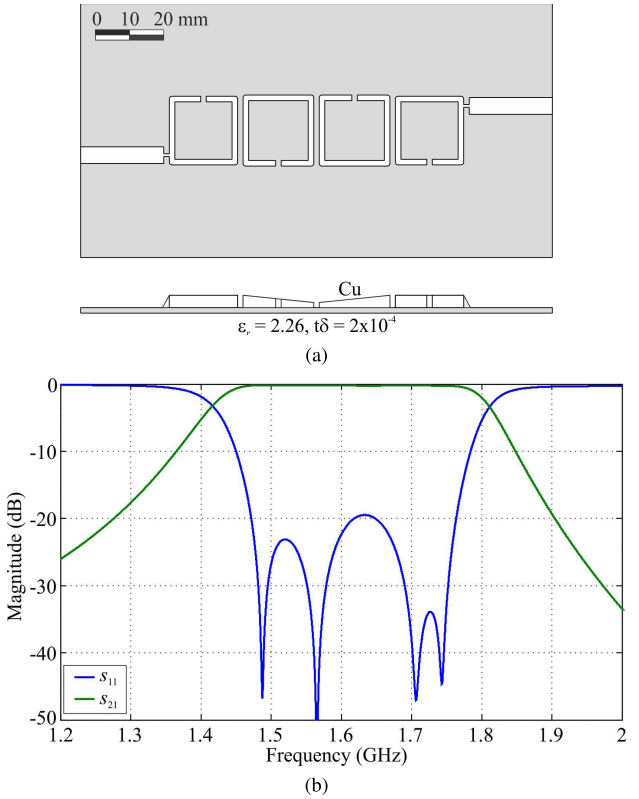

Fig. 9. (a) Top and lateral views of the layout of a fourth-order bandpass filter formed by coupled 3-D SRRs with variable sizes and height, whereas the width of SRR gaps and the distance between adjacent resonators are fixed. (b) Simulated reflection (s_{11}) and transmission (s_{21}) responses of the filter assuming SRRs are made of copper and placed on a substrate with $\epsilon_r = 2.26$ and $\tan\delta = 2 \times 10^{-4}$.

permitting the designer to place any features closer together than 1.6 mm. This filter model derives from those described already by employing 3-D SRRs, but in this case, both the width of the SRR gaps and the distance between adjacent filter elements are fixed at this minimum feature size. The overall size of the resonators and their height is the only adjustable design parameters used to tune the filter response. Once again, we use the case of copper SRRs on a low loss dielectric substrate as a comparison. We have found that the required level of coupling, for the chosen fixed distance between the resonators, can be achieved only if the walls of adjacent resonators have similar heights. Different configurations can fulfill this requirement; one possible layout, shown in Fig. 9(a), is formed by using a pair of central SRRs with a sloped top profile degrading from a height of 3.6 mm at the sides facing the external SRRs to 2 mm at the center so as to modulate the level of coupling in different sections. The simulated reflection and transmission coefficients of this filter, shown in Fig. 9(b), exhibit characteristics similar to those of the filter with 2-mm-thick SRRs whose response is reported in Fig. 8(c).

A third filter model made of raised SRRs with bandpass response centered at 2.45 GHz, shown in Fig. 10, has been adapted from an initial thin microstrip design employing convoluted SRRs, aiming for a more compact configuration. The specifications for the microstrip filter were as follows: passband width of $\simeq$100 MHz, maximum passband attenuation

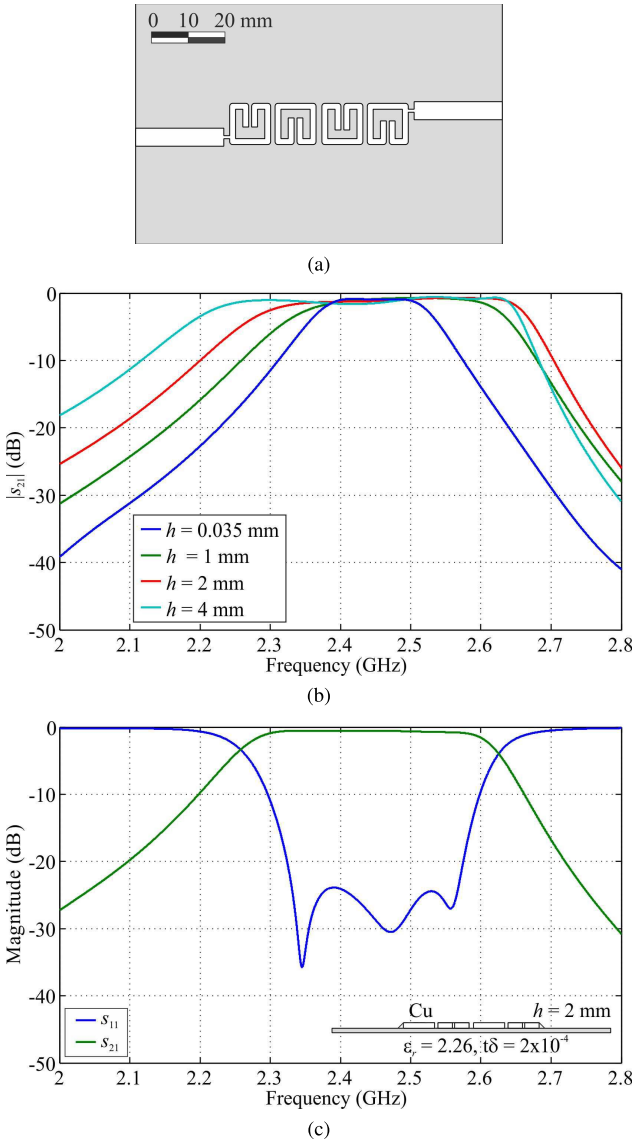

Fig. 10. Fourth-order bandpass filter employing coupled convoluted SRRs with center frequency at 2.45 GHz. The SRRs here are assumed to be made of copper (Cu) and printed on a substrate with $\epsilon_r = 2.26$ and $\tan\delta = 2 \times 10^{-4}$. (a) General layout. (b) Transmission coefficient (s_{21}) of the reference thin PCB design ($h = 0.035$ mm) as simulated with CST MWS and its modification as a result of raising the height of resonators while all other filter dimensions are kept fixed. (c) Reflection (s_{11}) and transmission (s_{21}) coefficients of a 3-D version of this filter with 2-mm-high resonators after reoptimization to restore the specified maximum insertion loss of 1 dB. Inset shows the lateral view of the 3-D filter variant.

of 1 dB, and stopband attenuation of 20 dB with stopband width of 400 MHz (i.e., width of transition bands $\simeq$150 MHz). The same 1.6-mm-thick ground backed polyethylene substrate is used as for the previous designs. This leads to the compact SRRs having side length $L = 11.15$ mm for a conductor track width $w = 1.6$ mm. The gap width of all resonators has been selected to be 0.8 mm, with interelement spacing of 1.8 mm at the center and 0.9 mm between the inner and outer SRRs. The layout of the reference filter model with planar copper SRR elements ($h = 0.035$ mm) and its transmission coefficient (s_{21}) are shown in Fig. 10(a) and (b), respectively; in Fig. 10(b) are also included the transmittance curves of the filter simulated for variable resonator height, with all other filter dimensions

unmodified, to illustrate the effect of bandwidth enlargement provided by the stronger coupling between the raised version of convoluted SRRs.

A 3-D filter having substantially the same footprint and layout but using raised square SRRs has been derived from the reference microstrip model by thickening the tracks to $h = 2$ mm and adjusting the position of tap lines, the widths of SRR gaps, and the interelement spacings to reoptimize its performance. The response of this filter with thick SRRs has been analyzed for both sets of reference and printed material combinations listed in Table II. The simulated reflection and transmission responses of the 3-D compact SRR filter model for the case of copper resonators and low loss polyethylene substrate are shown in Fig. 10(c). By comparing Fig. 10(b) and Fig. 10(c), it is clear that the filter with the 2-mm-high SRRs exhibits a much wider passband width (about three times larger) than the version with planar resonators, while rolloff characteristics outside the passband are similar. A comparison of the performance indices of the different filters developed is provided in Table III.

IV. 3-D Printed Filter Prototyping and Measurement

Two prototypes of the coupled 3-D SRR sample filters presented in Section III have been made on the V8 DDM printing platform coprinting thermoplastics and conductive ink [19]. One of the nozzles deposits the V8 ambiphillic silver ink, whose flow is controlled by an on-board pneumatic system. As mentioned in the Introduction, this conductive ink can be printed and cured at room temperature. The second nozzle is used for standard FDM of polymer filaments. The size of the nozzle, which is 0.25 mm, determines the maximum printing resolution, as no particular strategy is applied in the fabrication to exceed this limit (such as, for example, the technique of stretching the extruded ink to print fibers with resolution finer than the nozzle diameter described in [27]). However, an additional constraint exists for the minimum horizontal air gaps between conductor traces that our 3-D printer could be able to print reliably, which needs to be larger than 0.475 mm; following a conservative approach, we have assumed the minimum trace spacing and gaps width to be 0.8 mm, as in the designs shown in Section III.

In respect of the dielectric properties of the printed plastic structures, it is well-known that FDM objects are not printed as solids but as partially empty structures according to variable 3-D printing infill patterns with air voids, with the exception of external walls. Infill density, i.e., the amount of filament printed inside the object, directly relates to the strength, weight and printing duration, but also provides an obvious method for controlling the permittivity and loss tangent of a substrate [28]. As a result, while the permittivity of fully dense PLA is nominally $\epsilon_r = 2.75$ and its loss tangent $\tan\delta = 0.015$, lower values of dielectric constant can be achieved by adjusting the air infill volume fraction in the printed structure. This will also lower the effective loss tangent of the structure. An estimate of the dielectric parameters against the infill density can be obtained by Maxwell Garnett (MG) homogenization formulas [29]–[31].

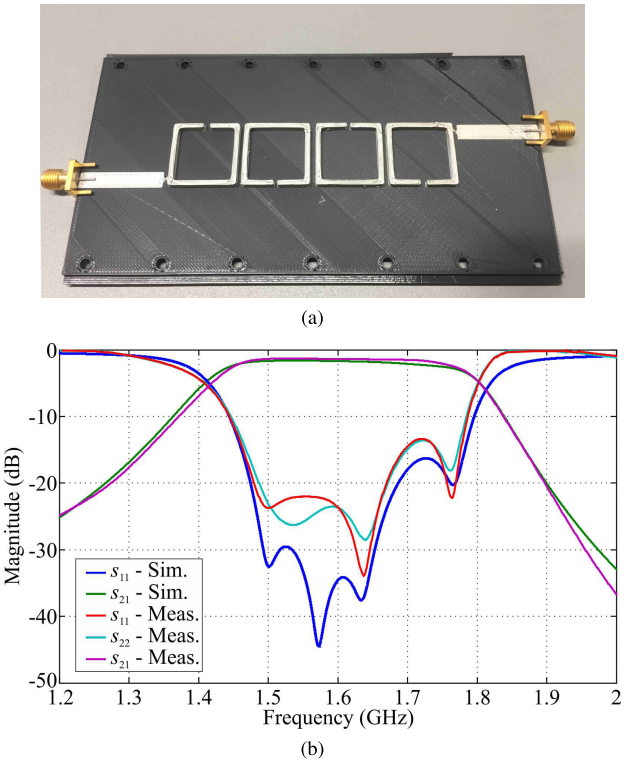

Fig. 11. (a) 3-D printed prototype of the 2-mm-high SRR bandpass filter with center frequency at 1.6 GHz. (b) Measured reflection and transmission coefficients of the filter compared with corresponding simulation results.

For all our prototypes, ground planes for the filters are formed by conductive aluminum tape. This was not essential, but a choice made to reduce printing times and the usage of silver ink. The SMA-to-microstrip connectors interfacing the filter feed lines to the coaxial cables for measurements were connected to the circuit by conductive epoxy. The realized prototype of the fourth-order bandpass filter with center frequency at 1.6 GHz, shown in Fig. 11(a), is made by 2-mm-high SRRs. While 4 mm thickness would offer a better performance, the 3-D printing equipment we have used has a technical limitation related to the size of the syringe containing the conducting ink; the available quantity of ink might have not been sufficient to complete a 4-mm structure, and therefore, we opted for fabricating 2-mm-high devices.

The dielectric substrate of the filter was printed with PLA filament with an infill density of 70% to target the desired design permittivity of 2.26, with the resulting loss tangent estimated to be 0.01 (see Table II).

The response of the filter was characterized by measuring its reflection and transmission coefficients with a vector network analyzer (VNA). A full two-port calibration of the VNA together with the coaxial cables and adapters used to connect the filter was performed to isolate the filter response. The results are shown in Fig. 11(b) in comparison with the corresponding simulation results taking into account the characteristics of printed materials. The measured s_{11} and s_{21} are in good agreement with numerical simulations and confirm the predicted wide bandwidth of the filter, which is more than two times larger than that of a planar microstrip filter with the same footprint. With respect to Fig. 8(c), it can also be

noted that the larger losses associated with the metallic and dielectric materials used in DDM determine some deterioration of the filter characteristics in the passband, yet the worsening of the attenuation performance is limited to about 1 dB. The increase in passband attenuation is close to the simulated values, which confirms the estimation of the printed PLA loss tangent based on the infill density and MG theory. Cross correlating simulation and measurement results, losses in the PLA substrate can be appraised to contribute to about 60% of the overall loss increment, which, in turn, means that by just making use of a lower loss 3-D printed substrate could considerably mitigate the additional passband loss.

A second prototype was manufactured based on the design for the fourth-order bandpass filter with center frequency at 2.45 GHz once again employing 2-mm-high compact SRRs of the form shown in Fig. 10(a). The same materials and printing settings as for the filter prototype described above have been used. This prototype is shown in Fig. 12(a).

The response of the filter measured with a VNA after a full two-port calibration is shown in Fig. 12(b) along with the scattering parameters simulated by using the printed material parameters. Measured s_{11}, s_{21}, and s_{22} exhibit similar passband width and rolloff characteristics as those of the numerical model. This confirms the substantial improvement in bandwidth achievable by using raised resonators rather than standard PCB construction. Passband attenuation in the real filter is in good agreement with that predicted by simulations, which suggests that also at these frequencies, the loss tangent of the printed PLA should be close to the value estimated based on the infill fraction. Measurements at 10 GHz via the Nicholson–Ross–Weir method [29], [32] showed that the fabricated PLA had as expected $\epsilon_r = 2.35$ and $\tan\delta < 0.02$. Some frequency shift was present between the fabricated filter and the model—inspection of the fabricated resonators showed that some fabrication errors were present, in particular, the sizes of the gaps of all resonators have been measured to be approximately 18% larger on average (the printed gaps tend to slightly expand toward the external part of the rings) than the nominal value of 0.8 mm, while the SRRs are marginally smaller overall than their nominal size. Simulations have shown that such larger gaps and smaller SRRs can, indeed, be responsible for the observed shift of the filter response, as illustrated by the comparison in Fig. 12(c) between measurements and the simulated results for the filter model amended to reflect the main dimensional deviations in the printed layout. Minor variations from the nominal design parameters were also detected in the spacings between the SRRs and in the transmission and tap lines widths, which contribute to both the observed slight mismatch of the impedance and narrowing of the passband. It is also apparent that the reflection coefficients at the two ports of the filter are less symmetric than in the prototype working at lower frequency. Generally, because of the smaller scale structure, the higher frequency filter is more sensitive to imperfections and granularities of the extruded conductors, as well as to the local variability of the patterned 3-D printed dielectric substrate. While in the S-band, these effects still have a minor impact on filter performance, 3-D printing for filters at higher frequencies requires higher resolution and

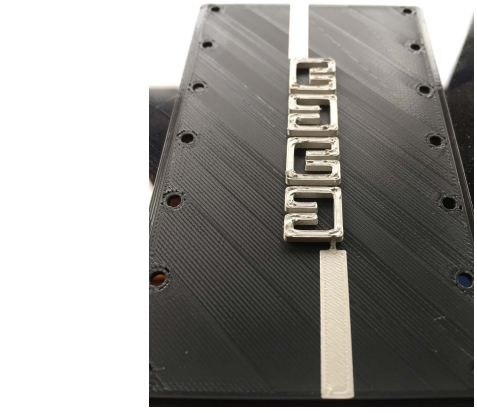

(a)

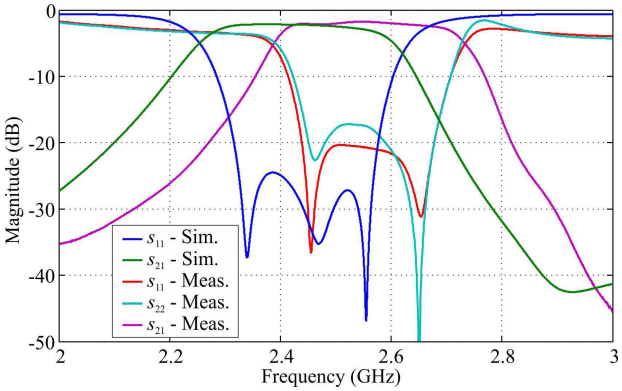

(b)

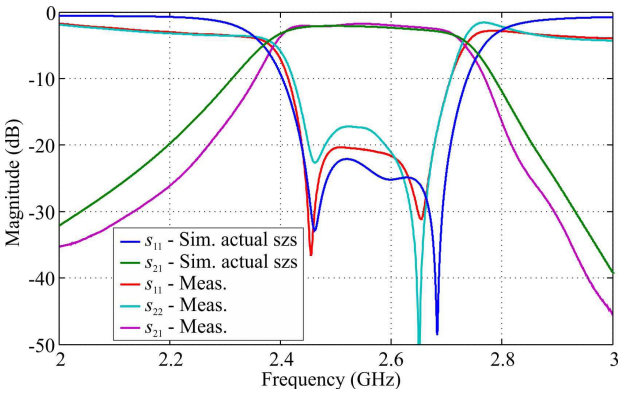

(c)

Fig. 12. (a) 3-D printed prototype of the 2-mm-high compact SRR bandpass filter with center frequency at 2.45 GHz. Measured reflection and transmission coefficients of the filter are compared with corresponding simulation results for: (b) nominal filter design; (c) filter model modified to take into account the main dimensional inaccuracies in the printed filter, namely, the actual gaps and SRR sizes.

fidelity than was achieved here. Finally, by comparing with Fig. 10(c), the increase in passband attenuation caused by the lossier conducting and dielectric printed materials can be seen to be on the order of 2 dB, which is greater than in the first filter prototype likely due to both the higher frequency band of operation and the compact and convoluted shape of resonators involving stronger localized electric fields and, thus, larger dielectric losses. In fact, the PLA substrate is estimated to account for about 65% of losses increase, the rest being instead associated with the reduced conductivity

of the 3-D printable conductor employed compared to pure copper. Other, lower loss FDM materials are already, or might shortly become, available, including blends of PC and ABS ($\tan\delta = 0.0055$) and PTFE ($\tan\delta = 0.0016$) [33]; the use of the latter would dramatically reduce dielectric losses, making them almost negligible with respect to those in the V8 printed conductors, and limiting the loss increase to be about 1 dB at these frequencies. Hence, low loss printable dielectrics are essential for future improvements.

In this regard, it is also worthy of note that very low permittivity and loss tangents are possible for very low density printed substrates [28]. Alternatively, paying attention to where in a structure the dielectric losses arise, and removing lossy materials from only that location could allow much higher performance with the same low performance materials. If one were to create a well directly below the gap in each split ring, the strongest electric fields would be in low loss air and not high loss substrates. This kind of substrate engineering offers further benefits from the 3-D fabrication method.

V. Conclusion

This article details our exploration of the potential offered by 3-D printing fabrication for future RF filter design and optimization. Using just the additional degree of freedom provided by building structures of differing heights, we have been able to reduce the resolution requirements for accurate filter production as compared to traditional thin PCB variants. Taking a thin PCB-based filter as a baseline, we have been able to show, using simulations and measurements, that greater coupling may be achieved through raising the height of resonators (up to three times greater depending on orientation). This is hugely beneficial as there are hard limits imposed by most fabrication methods on the minimal distance at which structures may be fabricated. Thick filter structures offer greater bandwidth, due to higher coupling, and also improved Q factors than equivalent size PCB variants.

We have demonstrated these benefits through the two 3-D printed test specimens fabricated on PLA substrates with ambiphilic silver ink for 1.6 and 2.45 GHz. Measurements of the fabricated 3-D filter prototype operating at the lower frequency have been found to be in good agreement with performance predicted by simulations; however, the samples of the higher frequency filter were noticed to be more sensitive to imperfections of the fabrication process because of their smaller scale challenging the accuracy and resolution of the available printer.

While our use of the third dimension to enhance coupling is a relatively simple one, it points to the great potential offered by facile 3-D fabrication techniques. Future advancements will include the development of complex 2-D and 3-D filtering structures, for example, by folding and stacking planar objects, to address advanced miniaturization and more sophisticated control of the electromagnetic performance

References

[1] E. S. Rosker, R. Sandhu, J. Hester, M. S. Goorsky, and J. Tice, "Printable materials for the realization of high performance RF components: Challenges and opportunities," *Int. J. Antennas Propag.*, vol. 2018, Jan. 2018, Art. no. 9359528. [Online]. Available: https://www.hindawi.com/journals/ijap/2018/9359528/

[2] Y. Lee *et al.*, "Rapid prototyping of ceramic millimeterwave metamaterials: Simulations and experiments," *Microw. Opt. Technol. Lett.*, vol. 49, no. 9, pp. 2090–2093, Sep. 2007. [Online]. Available: https://onlinelibrary.wiley.com/doi/abs/10.1002/mop.22697

[3] C. R. Garcia *et al.*, "3D printing of anisotropic metamaterials," *Prog. Electromagn. Res.*, vol. 34, pp. 75–82, 2012. [Online]. Available: http://www.jpier.org/pierl/pier.php?paper=12070311

[4] Y. Urzhumov, N. Landy, T. Driscoll, D. Basov, and D. R. Smith, "Thin low-loss dielectric coatings for free-space cloaking," *Opt. Lett.*, vol. 38, no. 10, pp. 1606–1608, May 2013. [Online]. Available: https://www.osapublishing.org/ol/abstract.cfm?uri=ol-38-10-1606

[5] L. Schulwitz and A. Mortazawi, "A compact millimeter-wave horn antenna array fabricated through layer-by-layer stereolithography," in *Proc. IEEE Antennas Propag. Soc. Int. Symp.*, Jul. 2008, pp. 1–4.

[6] P. T. Timbie, J. Grade, D. van der Weide, B. Maffei, and G. Pisano, "Stereolithographed MM-wave corrugated horn antennas," in *Proc. Int. Conf. Infr., Millim., THz. Waves*, Oct. 2011, pp. 1–3.

[7] C. C. Njoku, W. G. Whittow, and J. C. Vardaxoglou, "Microstrip patch antennas with anisotropic and diamagnetic synthetic heterogeneous substrates," *IEEE Trans. Antennas Propag.*, vol. 63, no. 7, pp. 3280–3285, Jul. 2015.

[8] J. W. Allen and B.-I. Wu, "Design and fabrication of an RF GRIN lens using 3D printing technology," *Proc. SPIE*, vol. 8624, Mar. 2013, Art. no. 86240V.

[9] M. Liang, W. R. Ng, K. Chang, K. Gbele, M. E. Gehm, and H. Xin, "A 3-D Luneburg lens antenna fabricated by polymer jetting rapid prototyping," *IEEE Trans. Antennas Propag.*, vol. 62, no. 4, pp. 1799–1807, Apr. 2014.

[10] F. Castles *et al.*, "Microwave dielectric characterisation of 3D-printed $BaTiO_3$/ABS polymer composites," *Sci. Rep.*, vol. 6, Mar. 2016, Art. no. 22714. [Online]. Available: https://www.nature.com/articles/srep22714

[11] B. Sanz-Izquierdo and E. A. Parker, "3-D printing of elements in frequency selective arrays," *IEEE Trans. Antennas Propag.*, vol. 62, no. 12, pp. 6060–6066, Dec. 2014.

[12] B. M. Turki *et al.*, "Significant factors in the inkjet manufacture of frequency-selective surfaces," *IEEE Trans. Compon., Packag., Manuf. Technol.*, vol. 6, no. 6, pp. 933–940, Jun. 2016.

[13] B. Zhang and H. Zirath, "3D printed iris bandpass filters for millimetre-wave applications," *Electron. Lett.*, vol. 51, no. 22, pp. 1791–1793, Oct. 2015.

[14] C. Guo, X. Shang, J. Li, F. Zhang, M. J. Lancaster, and J. Xu, "A lightweight 3-D printed X-band bandpass filter based on spherical dual-mode resonators," *IEEE Microw. Wireless Compon. Lett.*, vol. 26, no. 8, pp. 568–570, Aug. 2016.

[15] J.-S. Hong and M. J. Lancaster, *Microstrip Filters for RF/Microwave Applications*, 2nd ed. Hoboken, NJ, USA: Wiley, 2011.

[16] A. Vallecchi, C. J. Stevens, and E. Shamonina, "3D coupled resonators for enhanced filter design," in *Proc. 12th Eur. Conf. Antennas Propag. (EuCAP)*, Apr. 2018, pp. 1–4.

[17] E. MacDonald *et al.*, "3D printing for the rapid prototyping of structural electronics," *IEEE Access*, vol. 2, pp. 234–242, 2014.

[18] S.-Y. Wu, C. Yang, W. Hsu, and L. Lin, "3D-printed microelectronics for integrated circuitry and passive wireless sensors," *Microsyst. Nanoeng.*, vol. 1, Jul. 2015, Art. no. 15013. [Online]. Available: https://www.nature.com/articles/micronano201513

[19] S. B. Walker and J. A. Lewis, "Reactive silver inks for patterning high-conductivity features at mild temperatures," *J. Amer. Chem. Soc.*, vol. 134, no. 3, pp. 1419–1421, Jan. 2012. doi: 10.1021/ja209267c.

[20] Y. Xie *et al.*, "Microwave metamaterials made by fused deposition 3D printing of a highly conductive copper-based filament," *Appl. Phys. Lett.*, vol. 110, no. 18, May 2017, Art. no. 181903. [Online]. Available: https://aip.scitation.org/doi/full/10.1063/1.4982718

[21] D. Espalin, D. W. Muse, E. MacDonald, and R. B. Wicker, "3D Printing multifunctionality: Structures with electronics," *Int. J. Adv. Manuf. Technol.*, vol. 72, no. 5, pp. 963–978, May 2014. doi: 10.1007/s00170-014-5717-7.

[22] D. V. Isakov, Q. Lei, F. Castles, C. J. Stevens, C. R. M. Grovenor, and P. S. Grant, "3D printed anisotropic dielectric composite with meta-material features," *Mater. Des.*, vol. 93, pp. 423–430, May 2016. [Online]. Available: https://www.sciencedirect.com/science/article/pii/S0264127515310340

[23] J. Castro, E. A. Rojas-Nastrucci, A. Ross, T. M. Weller, and J. Wang, "Fabrication, modeling, and application of ceramic-thermoplastic composites for fused deposition modeling of microwave components," *IEEE Trans. Microw. Theory Techn.*, vol. 65, no. 6, pp. 2073–2084, Jun. 2017.

[24] T. C. Edwards and M. B. Steer, *Foundations for Microstrip Circuit Design*. Hoboken, NJ, USA: Wiley, 2016.

[25] E. Tatartschuk, N. Gneiding, F. Hesmer, A. Radkovskaya, and E. Shamonina, "Mapping inter-element coupling in metamaterials: Scaling down to infrared," *J. Appl. Phys.*, vol. 111, no. 9, May 2012, Art. no. 094904. doi: 10.1063/1.4711092.
[26] S. B. Cohn, "Direct-coupled-resonator filters," *Proc. IRE*, vol. 45, no. 2, pp. 187–196, Feb. 1957.
[27] H. Yuk and X. Zhao, "A new 3D printing strategy by harnessing deformation, instability, and fracture of viscoelastic inks," *Adv. Mater.*, vol. 30, no. 6, Feb. 2018, Art. no. 1704028. [Online]. Available: https://onlinelibrary.wiley.com/doi/abs/10.1002/adma.201704028
[28] S. Zhang, C. C. Njoku, W. G. Whittow, and J. C. Vardaxoglou, "Novel 3D printed synthetic dielectric substrates," *Microw. Opt. Technol. Lett.*, vol. 57, no. 10, pp. 2344–2346, Oct. 2015. [Online]. Available: https://onlinelibrary.wiley.com/doi/abs/10.1002/mop.29324
[29] A. M. Nicolson and G. F. Ross, "Measurement of the intrinsic properties of materials by time-domain techniques," *IEEE Trans. Instrum. Meas.*, vol. IM-19, no. 4, pp. 377–382, Nov. 1970.
[30] E. Massoni *et al.*, "Characterization of 3D-printed dielectric substrates with different infill for microwave applications," in *Proc. IEEE MTT-S Int. Microw. Workshop Series Adv. Mater. Processes RF THz Appl. (IMWS-AMP)*, Jul. 2016, pp. 1–4.
[31] L. Lewin, "The electrical constants of a material loaded with spherical particles," *J. Inst. Elect. Eng.–Part III: Radio Commun. Eng.*, vol. 94, no. 27, pp. 65–68, Jan. 1947.
[32] W. B. Weir, "Automatic measurement of complex dielectric constant and permeability at microwave frequencies," *Proc. IEEE*, vol. 62, no. 1, pp. 33–36, Jan. 1974.
[33] P. I. Deffenbaugh, R. C. Rumpf, and K. H. Church, "Broadband microwave frequency characterization of 3-D printed materials," *IEEE Trans. Compon., Packag., Manuf. Technol.*, vol. 3, no. 12, pp. 2147–2155, Dec. 2013.

Andrea Vallecchi received the Laurea (M.Sc.) degree *(summa cum laude)* in electronic engineering from the University of Florence, Florence, Italy, and the Ph.D. degree in information engineering, applied electromagnetics, and telecommunications from the University of Salerno, Salerno, Italy.

He was a Research Associate with the Laboratory of Antennas and Microwaves, University of Florence. In 2008, he joined the University of Siena, Siena, Italy, as a Post-Doctoral Research Fellow. In 2013, he was awarded a Marie Curie Research Fellowship with the University of Sheffield, Sheffield, U.K. He is currently with the Department of Engineering Science, University of Oxford, Oxford, U.K., and a Tutorial Lecturer of St. Hughs College, Oxford. His current research interests include the theoretical modeling and design of metamaterials, metasurfaces, and metamaterial-inspired antennas for applications at microwaves, terahertz, and optical frequencies.

Dr. Vallecchi was a co-recipient of the Best Antenna Theory Paper Award at the 8th European Conference on Antennas and Propagation in 2014. He has been a Visiting Research Fellow with the Queens University of Belfast, Belfast, U.K., on several occasions, and a Visiting Researcher with the University of California, Irvine, USA, in 2009.

Darren Cadman was born in Wolverhampton, U.K., in 1975. He received the Ph.D. degree from the Institute of Microwaves and Photonics, University of Leeds, Leeds, U.K., in 2003, that investigated the optical control of microstrip electromagnetic bandgap structures.

In 2007, he was with Filtronic Compound Semiconductors Ltd., where he took up the post of managing the Innovative Electronics Manufacturing Research Center based at Loughborough University, Loughborough, U.K. In 2016, he took up the post of Program Manager for the U.K.'s EPSRC funded project Synthesizing 3-D Metamaterials for RF, microwave and terahertz applications led by Loughborough University. His current research interests include the application of additive manufacturing processes to create microwave passive componentry.

William G. Whittow (M'12–SM'12) received the B.Sc. degree in physics and the Ph.D. degree in computational electromagnetics from the University of Sheffield, Sheffield, U.K., in 2000 and 2004, respectively.

From 2004 to 2012, he was a Research Associate with Loughborough University, Loughborough, U.K. In 2012, he became a Lecturer of electronic materials integration with the University of Loughborough. He became a Senior Lecturer in 2014 and a Reader (Associate Professor) of radio frequency materials in 2018 with the Wolfson School of Mechanical, Electrical and Manufacturing Engineering, Loughborough University. He has authored more than 215 peer-reviewed journal and conference articles in topics related to electromagnetic materials, synthetic dielectrics, dielectric measurements, 3-D-printing, wearable antennas, VHF antennas, specific absorption rate, FDTD, specific absorption rate, metamaterials, heterogeneous substrates, embroidered antennas, inkjet printing, electromagnetic compatibility, RFID tags, phantoms and genetic algorithms. His academic journal articles can be freely downloaded via: http://publications.lboro.ac.U.K./publications/all/collated/elwgw.html.

Dr. Whittow was the Coordinating Chair of the Loughborough Antennas and Propagation Conference (LAPC) from 2007 to 2011. In 2017, he was the recipient of the Women in Engineering Men As Allies Award. He is an Associate Editor of *Electronics Letters*. He serves on the Technical Program Committees for several IEEE international conferences. He has been asked to give 13 invited conference presentations; a 4-day invited workshop on bioelectromagnetics and teach about dielectric measurements at the European School of Antennas.

John (Yiannis) Vardaxoglou (F'12) received the B.Sc. degree in mathematical physics and the Ph.D. degree in electronics with the University of Kent, Canterbury, U.K., in 1982 and 1985, respectively.

In 1988, he joined Loughborough University, Loughborough, U.K., as a Lecturer, where he was promoted to Senior Lecturer in 1992 and a Professor of wireless communications in 1998. He served as the Dean of the School of Electronic, Electrical and Systems Engineering, Loughborough University, from 2011 to 2012. He established the 30-year-old Wireless Communications Research (WiCR) Group, Loughborough University, and founded the Center for Mobile Communications Research (CMCR). He is the Director of the Symeta Research Centre, (www.symeta.co.U.K.) funded by an EPSRC Grand Challenge Award, researching in wide-ranging topics applicable to cutting-edge wireless communications technology. Symeta collaborates with many internationally leading companies and universities. He has served as a consultant to various industries, holds six patents and is the Technical Director of Antrum Ltd. He has attracted research funding from industry and has been awarded 18 EPSRC research grants. He has authored or coauthored more than 300 refereed journals and conference proceeding articles (with 6500 citations) and has written a book on FSS. His current research interests include metamaterial structures, additive manufacturing (3-D printing) for RF/micro/mm wave engineering.

Dr. Vardaxoglou was elected as a Fellow of the Royal Academy of Engineers in 2011. He was the Chairman of the Executive Committee of the IETs Antennas and Propagation Professional Network in the U.K. and chaired the IEEEs Distinguish Lecturer Program of the Antennas and Propagation Society (AP-S) for five years. He founded the Loughborough Antennas & Propagation Conference (LAPC), which has been running since 2005. He has chaired numerous IEE//IET events and has served on the Steering Committee of the European Conference on Antennas and Propagation, EuCAP. He was the General Chair of EuCAP '07. He was recently awarded a prestigious EPSRCs Grand Challenge 5M (FEC) Award: Synthesizing 3-D Metamaterials for RF, Microwave and THz Applications, (http://gow.epsrc.ac.U.K./NGBOViewGrant.aspx?GrantRef=EP/N010493/1).

Ekaterina Shamonina received the degree in physics from Moscow State University, Moscow, Russia, in 1993, and the Ph.D. and the Habilitation degrees in theoretical physics from the University of Osnabrück, Osnabrück, Germany, in 1998 and 2006, respectively.

She was a Visiting Scientist with the University of Campinas, Campinas, Brazil, in 1996 and 1998. In 2000, she was awarded the Seven-Year Emmy Noether Fellowship from the German Research Council (Deutsche Forschungsgemeinschaft). From 2000 to 2002, she spent the first leg of the fellowship with the University of Oxford, Oxford, U.K. After six months at Imperial College, London, U.K., she returned to the University of Osnabrück, where she built up a research group working on electromagnetic metamaterials. She was a Professor in advanced optical technologies with the University of Erlangen–Nuremberg, Erlangen, Germany, in 2008. She moved to Imperial College London, in 2011, as a Leverhulme Reader, and joined the University of Oxford, Oxford, U.K., in 2013, as a Professor of engineering science. She has authored or coauthored more than 200 refereed journals and conference proceeding articles (with 4200 citations) and 2 book chapters. She coauthored jointly with Professor Laszlo Solymar *Waves in Metamaterials* (Oxford Univ. Press, 2009) and edited the *Handbook of Metamaterials and Plasmonics* (World Sci., 2017; Vol. 1: Electromagnetic Materials). She is currently the Head of the OxiMeta, the Oxford Metamaterials Center, with more than 30 academics from engineering, materials, physics and medical sciences at Oxford and commercial partners. She is also a co-founder and a Director of the university spinout company Metaboards Ltd., developing metamaterial-based advanced wireless power and data technologies. Her main research interests apart from metamaterials have been amorphous semiconductors, photorefractive materials, antennas and plasmonics.

Dr. Shamonina was the recipient of the Hertha-Sponer Prize 2006 of the German Physical Society for pioneering work in electromagnetic metamaterials.

Christopher J. Stevens (M'16) received the Graduate degree (First Class Hons.) in physics from the University of Oxford, Oxford, U.K., in 1990, and the D. Phil. (Ph.D.) degree in condensed matter physics following a three-year doctoral degree course at the University of Oxford, in 1994.

He was with Uiversita Degli Studi di Lecce, Italy, where he was involved with the properties of wide bandgap semiconductor materials. He was a Post-Doctoral Fellow with the Clarendon Laboratory, where he was involved with the dynamic properties of high temperature superconductors, after which he held a Royal Academy of Engineering Fellowship at St Hugh's College, Oxford. During this period, he developed a number of novel devices based on kinetic inductance and photomixing effects. He is currently an Associate Professor of engineering science with the University of Oxford, and is a Fellow of St. Hugh's College, Oxford. His current research interests include ultra-wideband communications, metamaterials, ultrafast nanoelectronics, and high-speed electromagnetics.

Dr. Stevens was the recipient of several awards for practical physics.